Analytica Chimica Acta 1220 (2022) 339994

Contents lists available at ScienceDirect

Analytica Chimica Acta

journal homepage: www.elsevier.com/locate/aca

Carbon nanorods assembled coral-like hierarchical meso-macroporous carbon as sustainable materials for efficient biosensing and biofuel cell

Cuixing Xu [a,b], Gangyong Li [b,c], Ming Zhou [a,**], Zongqian Hu [b,*]

[a] Key Laboratory of Polyoxometalate and Reticular Material Chemistry of Ministry of Education, National & Local United Engineering Laboratory for Power Batteries, Key Laboratory of Nanobiosensing and Nanobioanalysis at Universities of Jilin Province, Analysis and Testing Center, Department of Chemistry, Northeast Normal University, Changchun, Jilin Province, 130024, PR China

[b] Beijing Institute of Radiation Medicine, Beijing, 100850, PR China

[c] Key Laboratory of Hunan Province for Advanced Carbon-based Functional Materials, School of Chemistry and Chemical Engineering, Hunan Institute of Science and Technology, Yueyang, 414006, Hunan, PR China

HIGHLIGHTS

- Cucumber was transformed into sustainable carbon materials for construction various bioelectrochemical deveies.
- The lactate biosensor exhibits excellent detection performance, and is eligible for the determination in real samples.
- The lactate biofuel cell with CN-CHMC exhibits high output power, and can harvest electrical energy from real samples.

GRAPHICAL ABSTRACT

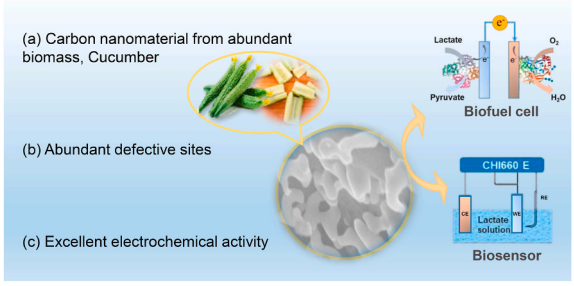

ARTICLE INFO

Keywords:
Cucumber
Sustainable
Lactate
Biosensor
Biofuel cell

ABSTRACT

Sustainable conversion of renewable biomass into high-performance electrode materials has attracted extensive scientific and technological attention. However, to our knowledge, the potential of biomass derived carbon in biosensors and biofuel cells (BFCs) developments remains to be explored. Herein, the carbon nanorods assembled coral-like hierarchical meso-macroporous carbon (CN-CHMC) was synthesized as a sustainable electrode material to construct biosensor and lactate/air BFC. The CN-CHMC from cucumber (*Cucumis sativus*) possesses porous structure and plentiful defects, which not only facilitate the effective immobilization of enzymes but also accelerate electron transfer on the bioelectrode surfaces. As an electrochemical lactate biosensor, the CN-CHMC-based biosensor exhibits a wider linear range with lower detection limit (3.6 μM) and higher sensitivities (57.18 and 30.99 μA mM^{-1} cm^{-2}) compared to carbon nanotube (CNT)-based biosensor. The feasibility of CN-CHMC-based biosensor in practical analysis is demonstrated by detecting lactate contents in real samples. By coupling with bilirubin oxidase-based biocathode, the lactate/air BFC equipped with CN-CHMC reveals a higher output power (112.7 μW cm^{-2}) than that of CNT-based BFC. More interestingly, the lactate/air BFC demonstrates the ability to harvest energy from multi-component samples. The application of CN-CHMC may provide a new avenue to synthesize electrode materials with economical cost and excellent electrochemical activity.

* Corresponding author.
** Corresponding author.
E-mail addresses: zhoum739@nenu.edu.cn (M. Zhou), huzongqian@hotmail.com (Z. Hu).

https://doi.org/10.1016/j.aca.2022.339994
Received 25 March 2022; Received in revised form 11 May 2022; Accepted 24 May 2022
Available online 31 May 2022

1. Introduction

As a dynamic metabolite in the anaerobic glycolysis, lactate is considered as a key marker for monitoring tissue oxidation and physical training levels of athletes [1,2]. Lactate levels can also be used as an indicator of fermentation, as well as the freshness and stability of products such as juices and milk [3,4]. Therefore, electrochemical biosensors for lactate determination are of paramount significance in food quality and clinical diagnosis due to their high sensitivity and specificity [2,5]. In addition, enzymatic biofuel cells (BFCs) can convert the chemical energy stored in the biosubstances into electrical energy through enzyme-based bioelectrocatalysis, and are considered as the next generation alternative energy sources [6,7]. As a common organic acid, lactate is the biosubstance of choice since it is readily available in daily products and biological fluids, and possesses a higher solubility in water (7.6 M) than other biofuels [4,7]. For lactate biosensor and BFC applications, lactate oxidase (LOx) can catalyze the conversion of lactate to pyruvate, which is usually preferred due to its favorable kinetics, high specificity, and relatively low cost [4,8]. However, the redox-active centers are buried in the insulating protein, rendering them inaccessible for effective electrical communication with bare electrodes [9]. Therefore, the effective electron transfer is of fundamental significance for the development of biosensors and BFC elements [10,11].

Nanomaterials have attracted considerable attention in the fields of energy storage conversion, catalysis and adsorption due to their large specific surface area, excellent electrical conductivity, and tunable physical/chemical properties [12–14]. Therefore, integrating nanomaterials on the electrode surfaces is expected to effectively accelerate the electron transfer while retaining function and activity of redox enzymes, which is of great significance for the development of bioelectrochemical devices [15,16]. Among the various types of nanomaterials for enzyme immobilization, carbon nanomaterials have mostly been investigated due to their favorable electrical conductivity, wide potential window, excellent chemical stability and good chemical inertness [17–20]. Recently, from the perspective of sustainability, biomass-derived carbon nanomaterials have fascinated the scientific fraternity owing to their multiple heteroatoms, low cost and ecofriendly synthetic process [21,22]. Besides the economic benefits from nature biomass, these materials also inherit the compatibility, high electronic conductivity, wide potential window and chemical inertness of traditional carbon nanomaterials [23,24]. These characteristics endow them with great potential as electrode materials for high-performance biosensors and BFCs constructions, but there are few reports in literature on this topic and further exploration is needed.

As a fast growing vegetable distributed in most countries of the world, the flesh part of the cucumber (*Cucumis sativus*) is mainly composed of a cellulose structure containing various minerals and vitamins, suggesting that cucumber can be transformed into porous material [25]. Therefore, a low-cost precursor (cucumber) is employed to fabricate carbon nanorods assembled coral-like hierarchical meso-macroporous carbon (CN-CHMC) as electrode material for immobilizing LOx to construct lactate biosensor and BFC. Physical characterization revealed that CN-CHMC possesses plentiful defects and porous structure, which can improve electron transfer rate and offer effective building blocks for high-quality enzyme loading. Consequently, as a biosensor for lactate, the CN-CHMC-based biosensor exhibits outstanding detection performance. In a semi-biofuel cell configuration, the CN-CHMC-based lactate/air BFC yields a higher output power. More importantly, the as-assembled lactate/air BFC has the ability to harvest energy from human sweat and soft drink.

2. Results and discussion

2.1. Characterization of the carbon nanorods assembled coral-like hierarchical meso-macroporous carbon (CN-CHMC)

The scanning electron microscopy (SEM) image of CN-CHMC witness a coral-like structure, which is assembled from many carbon nanorods with the diameter of ~100 nm (Fig. 1A). It is also obvious that CN-CHMC possesses a highly porous structure (represent by red rounds), which may offer effective building blocks for high-mass enzyme immobilization and favorable channels for the penetration and transportation of species [26,27]. The high-resolution transmission electron microscopy (HRTEM) image of CN-CHMC in Fig. 1B shows a distorted and defective surface, demonstrating the amorphous nature of the CN-CHMC. In addition, the element mapping images in Fig. 1C suggest the distributions of O and N over the CN-CHMC.

In Fig. 2A, the X-ray diffraction (XRD) pattern of CN-CHMC presents two broad weak peaks at ~24° and ~44°, corresponding to the (002) and (101) planes, respectively [28]. The weak peak is also an indication of the existence of amorphous structure on CN-CHMC [29]. For the Raman spectrum of CN-CHMC displayed in Fig. 2B, there are two obvious bands located at ~1359 cm^{-1} and ~1595 cm^{-1}, corresponding to D and G bands, respectively [30]. The former generally corresponds the existence of the defects/disordered carbon structure, while the latter corresponds to the E_{2g} phonon of stretching vibration of sp^2 C═C bond [31]. Moreover, the intensity ratio of the D to G bands (I_D/I_G) is employed to describe the extent of defects [32]. The I_D/I_G value of CN-CHMC (2.67) is higher than that of ordered mesoporous carbon (0.82) [32] and carbon nanotube (CNT, 0.74) [33]. The higher I_D/I_G value suggests that the CN-CHMC contains abundant defective sites, which may be propitious to accelerate electron transfer [34]. The nitrogen adsorption-desorption isotherms in Fig. 2C manifest the textural porosity of CN-CHMC. The Brunauer Emmett Teller (BET) surface area of CN-CHMC is calculated by the BET model to be 127.30 $m^2\ g^{-1}$. In addition, the Barrett-Joyner-Halenda (BJH) model is used to characterize the pore volume and pore size distribution of CN-CHMC [18]. The pore volume of CN-CHMC is 0.21 $cm^3\ g^{-1}$, which is calculated by taking the volume uptake at the relative pressure P/P_0 of 0.996. The pore size distribution of CN-CHMC in the inset of Fig. 2C reveals that the CN-CHMC contains a large number of mesopores (centered at 34 nm) and macropores (centered at 79 nm), which is consistent with SEM results. Such hierarchical meso-macroporous structure of CN-CHMC may be beneficial to the rapid penetration and transport of species and accordingly improve the electrochemical performance [35,36].

Fig. 2D shows the X-ray photoelectron spectroscopy (XPS) spectrum of CN-CHMC. The three elements (C, N and O) in CN-CHMC can be confirmed by the C 1s peak (284.61 eV, 87.12 at.%), N 1s peak (398.70 eV, 1.25 at.%) and O 1s peak (532.50 eV, 11.63 at.%), respectively (Fig. 2D) [37]. The O 1s spectrum of CN-CHMC in Fig. 2E shows three relatively weak peaks, corresponding to C═O (531.75 eV), C–OH/C–O–C (532.87 eV) and COOH (533.72 eV) groups of CN-CHMC [37,38]. In Fig. 2F, the N 1s spectrum of CN-CHMC is fitted into three individual peaks corresponding to pyridinic N (398.1 eV), pyrrolic N (400.2 eV) and graphitic N (401.8 eV) [39]. The existence of N in CN-CHMC may be conducive to providing more defect sites, and thus improve the electrochemical activity of CN-CHMC [40]. As revealed in Fig. S1, the Fourier transform infrared (FT-IR) spectrum of CN-CHMC shows two absorption bands at ~3453 cm^{-1} and 643 cm^{-1}, corresponding to O–H and C–H stretching vibrations, respectively [41]. The bands at ~1650 and ~1425 cm^{-1} are resulted from the N–H or C═C vibration and C–N vibration, respectively [18,38]. The XPS and FT-IR spectra demonstrate the existence of oxygen-containing functional groups (OFGs) in CN-CHMC. The OFGs can enhance the hydrophilicity of the material, which is beneficial to the immobilization of enzymes and thereduction of charge transfer resistance [26,42].

2.2. Electrochemical reactivity

In order to examine the electrochemical reactivity of CN-CHMC, potassium ferricyanide ($K_3Fe(CN)_6$), which is highly sensitive to the material surface, was selected as the electrochemical probe [27]. Fig. S2A exhibits the cyclic voltammograms (CVs) of different electrodes in 5 mM K_3 [$Fe(CN)_6$] including 0.1 M KCl. As shown, the potential separation (ΔE_p) between the oxidation and reduction peaks at CN-CHMC modified glassy carbon electrode (CN-CHMC/GCE, 68 mV) is much lower than that at CNT/GCE (74 mV) or bare GCE (85 mV), which suggests that the presence of CN-CHMC can make the electron transfer easier than that at CNT/GCE or bare GCE. According to the Randles-Sevcik equation [43], the CN-CHMC/GCE exhibits a larger electroactive surface area of 0.13 cm^2 compared to CNT/GCE (0.11 cm^2) or bare GCE (0.071 cm^2). Additionally, the electron-transfer properties of different electrodes were also evaluated using electrochemical impedance spectroscopy (EIS). The charge transfer resistance (*R*ct), which is directly related to the electron transfer efficiency between the electrode materials and electrolyte interface, can be obtained from the spectrum [36,44]. The Randles equivalent circuit (inset of Fig. S2B) is chosen to fit the obtained impedance data. By fitting the data (Fig. S2B), the CN-CHMC/GCE (63.6 Ω) shows a lower *R*ct value than that at CNT/GCE (137.8 Ω) or bare GCE (271.5 Ω). These results suggest that CN-CHMC can provide well electron pathway between the electrode and electrolyte and accordingly boost the electrochemical activity.

2.3. Electrochemical oxidation and detection of lactate

The development of enzymatic biosensors for selective and sensitive lactate quantification has been an important focus for research [5]. LOx, one of the most widely used enzymes, catalyses the oxidation of lactate to pyruvate coupled to the reduction of oxygen (O_2) to hydrogen peroxide (H_2O_2). Since the lactate concentration is proportional to O_2 consumption produced by the enzymatic reaction, the lactate concentration is determined by indirectly measuring the reduction response changes caused by O_2 consumption, which offers the advantage of excellent anti-interference ability from other electroactive species [8,45]. Here, the electrochemical activities of CN-CHMC-based lactate biosensor (CN-CHMC/LOx) and CNT-based biosensor (CNT/LOx) toward O_2 reduction reaction were firstly evaluated by recording the CVs in N_2- and Air-saturated PBS. As shown in Fig. 3A–B, a well-defined reduction current can be found in the air-saturated solution, while there is no faradaic current in N_2-saturated solution, suggesting that O_2 reduction reaction occurs at the two electrodes [46]. However, the reduction potential for the electroreduction of O_2 at CN-CHMC/LOx (−0.05 V) is more positive than that at CNT/LOx (−0.13 V). In addition, the catalytic reduction response at CN-CHMC/LOx is as high as −689.46 μA cm^{-2}, which is 2.21-fold larger than that at CNT/LOx. These results reflect that CN-CHMC/LOx can provide an enhanced electrocatalytic activity for O_2 reduction compared to CNT/LOx.

To investigate lactate oxidation catalyzed by LOx on CN-CHMC, the voltammetric responses of CN-CHMC/LOx were recorded in air-saturated PBS with various concentrations of lactate (0.5 and 1.0 mM lactate) (Fig. 3C). As displayed, the addition of lactate into solution results in an obvious decrease in the reduction response, which is caused by the O_2 reduction catalyzed by the CN-CHMC/LOx [47]. This decrease may be related to the occurrence of enzyme-catalyzed reaction between the LOx-flavin adenine dinucleotide (FAD) and lactate according to following equations [48]:

$$LOx - FAD + Lactate \leftrightarrow LOx - FADH_2 + Pyruvate \quad (1)$$

$$LOx - FADH_2 + O_2 \rightarrow LOx - FAD + H_2O_2 \quad (2)$$

The consumption of O_2 during enzyme-catalyzed reaction leads to the decrease in the concentration of O_2 in the electrolyte. Additionally, the reduction current is almost unchanged after the addition of 1.0 mM lactate into N_2-saturated solution, further confirming that the response generated by the addition of lactate is attributed to the O_2 in the buffer solution (Fig. S3). For comparison, similar measurements were conducted on the CNT/LOx (Fig. 3D). As shown, the reduction current of CNT/LOx gradually decreases with the increases of lactate concentration. However, the reduction current produced by lactate oxidation at CN-CHMC/LOx is more than twice higher than that at CNT/LOx (Table S1). This phenomenon may be explained that the porous

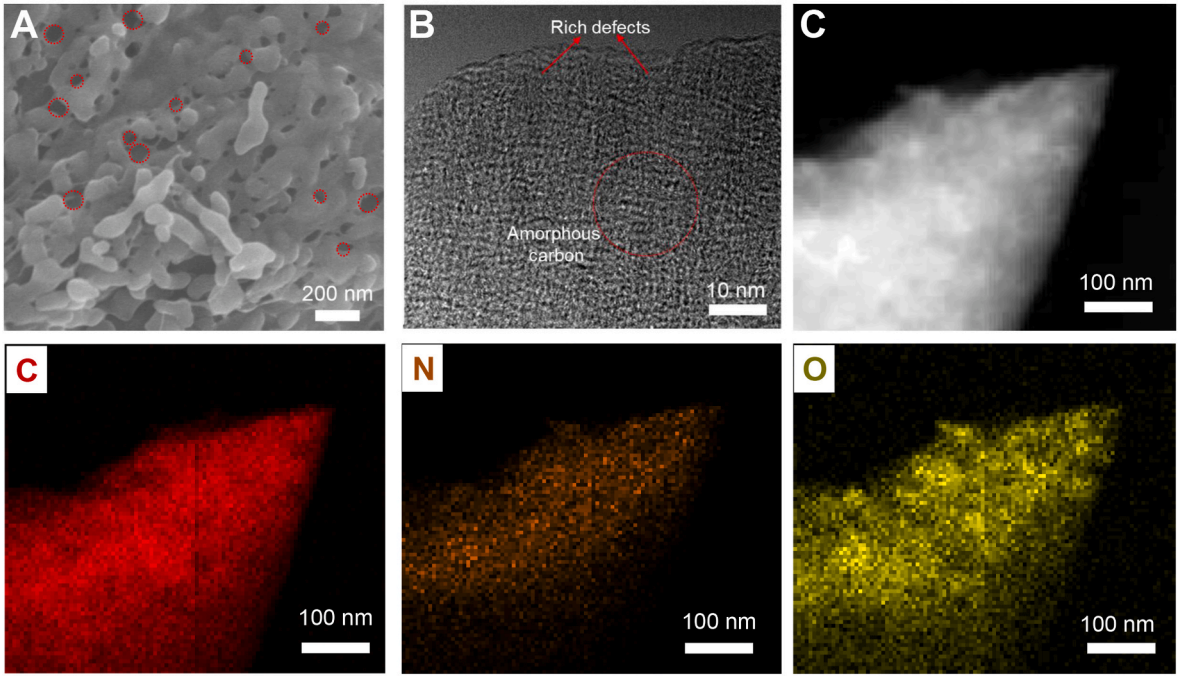

Fig. 1. (A) SEM image of CN-CHMC. (B) HRTEM image of CN-CHMC. (C) High-angle annular dark-field scanning TEM image of CN-CHMC and the corresponding element mapping images for C, O and N elements.

structure and abundant defect sites on CN-CHMC would be beneficial to the enhanced electron-transfer property between species and the nanomaterials.

In view of the outstanding electrocatalytic activity at CN-CHMC/LOx for lactate, CN-CHMC/LOx was used to detect lactate. Fig. 4A and B exhibits the typical current-time curves obtained at CN-CHMC/LOx and CNT/LOx upon the sequential additions of lactate into a magnetically stirred air-saturated PBS at −0.45 V. Such a low applied potential is beneficial to reduce possible interference and thus endow the lactate biosensor with a favorable selectivity [37]. As displayed, the injection of lactate into PBS causes a rapid decrease in the reduction current associated with the O_2 reduction. The corresponding calibration curves were displayed in Fig. 4C. As shown, the CN-CHMC/LOx exhibits two linear ranges of 20–580 μM ($R^2 = 0.999$) and 580–1280 μM ($R^2 = 0.997$). The corresponding sensitivities are 57.18 and 30.99 μA mM^{-1} cm^{-2}, respectively, which are higher than that obtained at CNT/LOx. The detection limit of 3.6 μM (S/N = 3) at CN-CHMC/LOx is 2.25 times lower than that at CNT/LOx. Table S2 summarizes the analytical performance of different LOx-based biosensors for lactate detection. As displayed, the detection performance of CN-CHMC/LOx is greatly superior to other electrochemical lactate biosensors reported in literature.

Small electroactive species have a tendency to be adsorbed on the electrode surface and subsequently oxidized or reduced, which may cause the risk of interference for lactate detection [49]. Thus, the effects of some possible biomolecules (uric acid (UA), acetaminophen (APAP), dopamine (DA), ascorbic acid (AA), glucose, and L-cysteine (L-cys)) on the amperometric responses of lactate were evaluated. In Fig. 4D, a distinct response is found for the addition of 1.0 mM lactate, while subsequent injections of interferences give rise to negligible current responses. The results indicate the high selectivity of CN-CHMC/LOx for lactate detection. To assess its long-term storage stability, the CN-CHMC/LOx was stored at 4 °C and employed to investigate the amperometric response for 1.0 mM lactate every three days (Fig. S4). The CN-CHMC/LOx electrode still retains 91.8% of its initial response after 15-day storage, which indicates the excellent storage stability of CN-CHMC/LOx.

The excellent biosensing performance and stability of CN-CHMC/LOx endow it with huge potential for the determination of lactate in real samples. To verify the feasibility, the CN-CHMC/LOx was applied to analyze the concentrations of lactate in human sweat and soft drink by adopting standard addition method. Prior to measurements, the soft drink was diluted 10-fold with deionized water. Lactate detection in real samples was carried out by injecting 0.04 mL of human sweat or diluted soft drink into a 5.0 mL of magnetically stirred air-saturated PBS. As shown in Table 1, the satisfactory recoveries between 96.7% and 103.3% indicate the great potential of the CN-CHMC/LOx for practical lactate analysis [37,50].

2.4. Characterization of lactate/air biofuel cell (BFC)

After immobilizing LOx and tetrathiafulvalene (TTF) onto CN-CHMC/GCE, the resulting CN-CHMC-based bioanode shows a superior electrocatalytic activity for lactate. Fig. 5A displays the CVs of CN-CHMC-based (CN-CHMC/LOx-TTF) and CNT-based bioanode (CNT/LOx-TTF) in the presence or absence of 50 mM lactate. As shown, there is a pair of distinct peaks located at ~0.10 V and ~0.20 V only in the absence of lactate, which is a representative redox wave of TTF/TTF^+ redox couple [51,52]. When lactate is present in the solution, the FAD of immobilized LOx can oxidize the lactate that diffuses into the enzyme layer to form pyruvate (S1), and the generated LOx ($FADH_2$) is further oxidized to LOx (FAD) by TTF^+ (S3).

$$LOx - FADH_2 + 2\,TTF^+ \rightarrow LOx - FAD + 2\,TTF + 2\,H^+ \quad (3)$$

Subsequently, the TTF generated by the above reaction is electrochemically reoxidized to TTF^+ ion on the electrode surface, producing an enhanced oxidation current (S4).

$$2\,TTF \rightarrow 2\,TTF^+ + 2\,e^- \quad (4)$$

The disappearance of the reduction peak is indicative of the fast regeneration rate of TTF from the reaction of TTF^+ and LOx ($FADH_2$) [52]. Therefore, it can be concluded that the enhanced oxidation current is related to the oxidation reaction of TTF triggered by LOx biocatalysis, indicating the occurrence of TTF-mediated bioelectrocatalytic process at CN-CHMC/LOx-TTF and CNT/LOx-TTF. However, the oxidation current for the electrooxidation of 50 mM lactate at CN-CHMC/LOx-TTF is much larger than that at CNT/LOx-TTF, which indicates that the CN-CHMC-based bioanode possesses a higher bioelectrocatalytic activity for lactate oxidation than CNT-based bioanode. The background-subtracted polarization curves in Fig. 5B further demonstrates that the electrochemical response for 50 mM lactate oxidation at

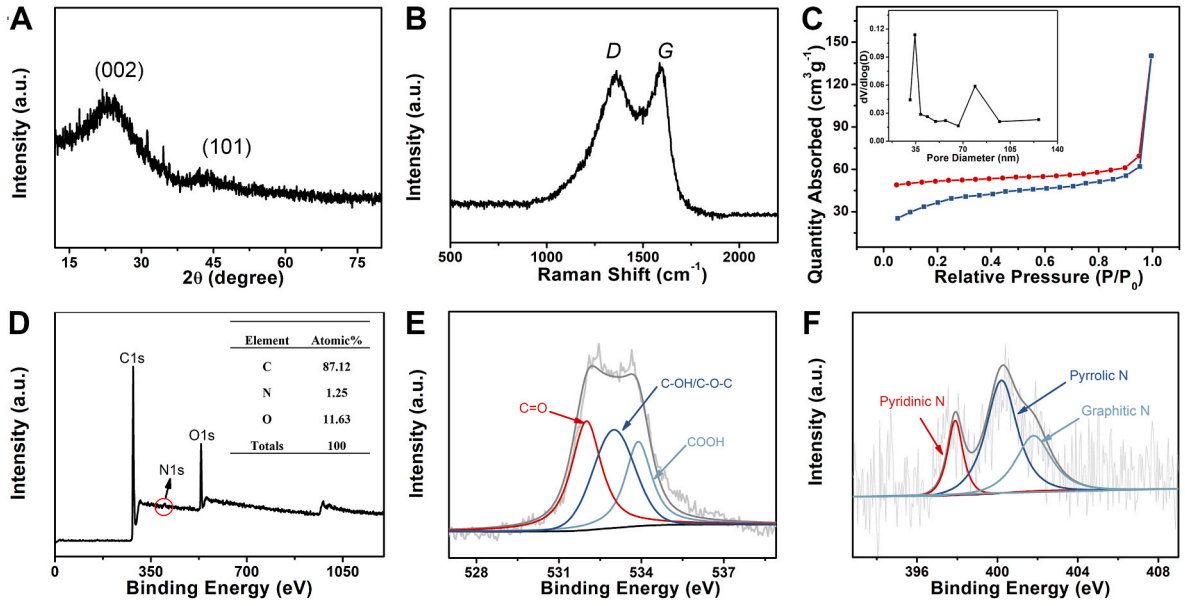

Fig. 2. (A) XRD pattern of CN-CHMC. (B) Raman spectrum of CN-CHMC. (C) Nitrogen adsorption desorption isotherm for CN-CHMC. Inset: Pore size distribution of CN-CHMC. (D) XPS spectrum of CN-CHMC. Inset: relative atom percentage. (E) High-resolution XPS spectrum of O 1s. (F) High-resolution XPS spectrum of N 1s.

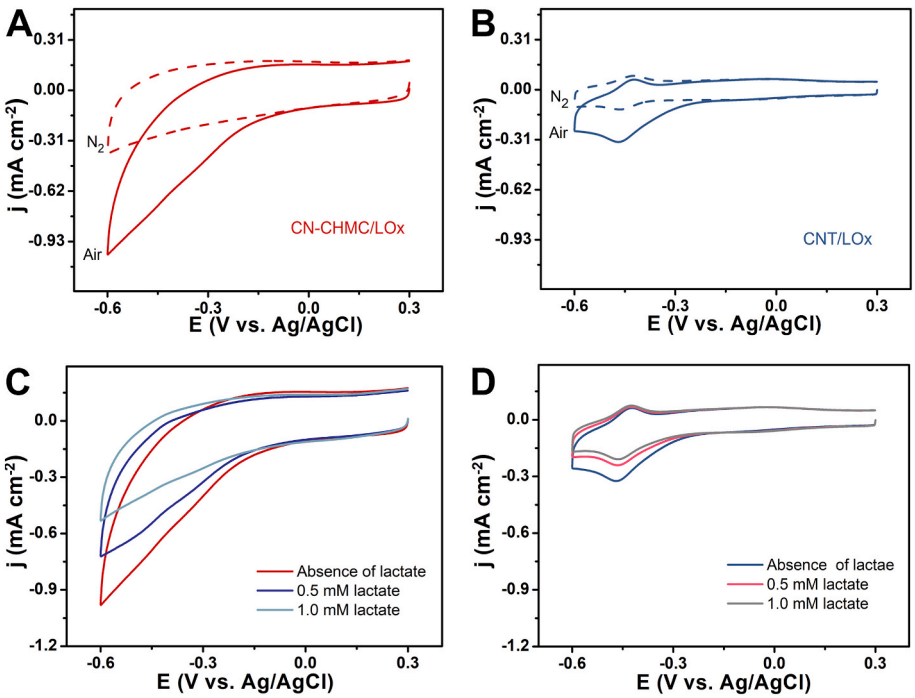

Fig. 3. (A) CVs of CN-CHMC/LOx in N_2-saturated and air-saturated 0.1 M pH 7.0 PBS. (B) CVs of CNT/LOx in N_2-saturated and air-saturated 0.1 M pH 7.0 PBS. (C) CVs of CN-CHMC/LOx in air-saturated 0.1 M pH 7.0 PBS with different lactate concentrations. (D) CVs of CNT/LOx in air-saturated 0.1 M pH 7.0 PBS with different lactate concentrations. Scan rate: 50 mV s^{-1}.

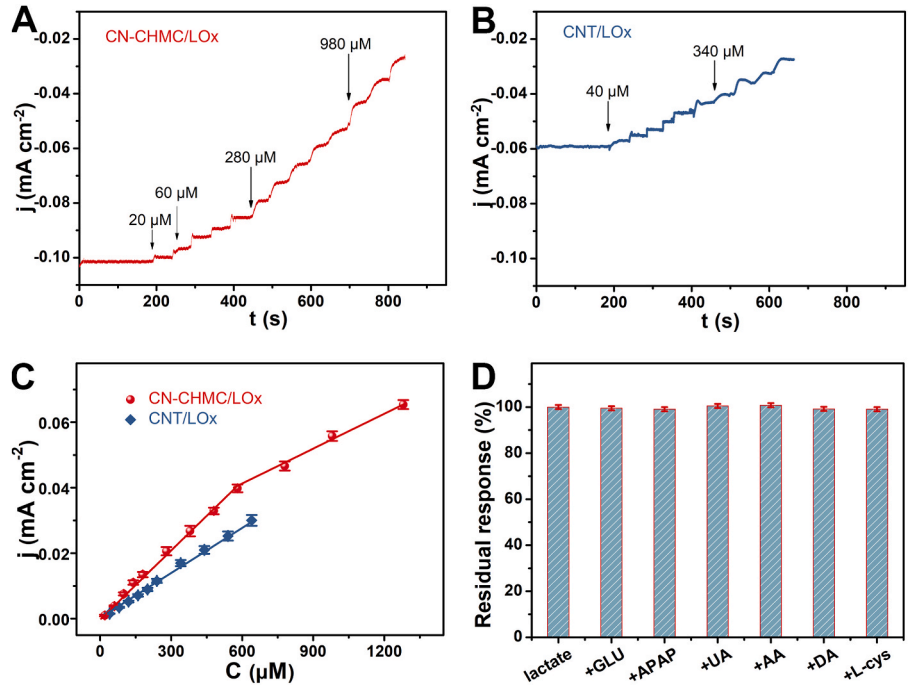

Fig. 4. (A) Current-time curve at CN-CHMC/LOx with the successive addition of lactate. (B) Current-time curve at CNT/LOx with the successive addition of lactate. (C) Calibration curves for lactate at CN-CHMC/LOx and CNT/LOx. (D) Current responses at CN-CHMC/LOx to the successive addition of 1.0 mM lactate, 0.1 mM interferents (glucose, APAP, UA, AA, DA and L-cys). Electrolyte: magnetically stirred air-saturated 0.1 M pH 7.0 PBS. Applied potential: −0.45 V.

CN-CHMC/LOx-TTF can reach 0.19 mA cm^{-2} at 0.30 V, which is larger than that at CNT/LOx-TTF (0.077 mA cm^{-2} at 0.30 V) under the same condition. It is predictable that employing CN-CHMC as support material may endow the constructed BFC with a favorable output power.

Bilirubin oxidase (BOx), a typical multicopper oxidase, is usually used as a cathodic biocatalyst to catalyze four-electron O_2 reduction under neutral condition [53]. Fig. 5C shows the CVs recorded at BOx-based biocathode in N_2 and air-saturated 0.1 M pH 7.0 PBS. As shown, the presence of O_2 introduces a pronounced catalytic current, while such catalytic phenomenon is not observed in the absence of O_2. As can be observed from the polarization curves in Fig. 5B, the catalytic current commenced at about +0.54 mV (vs. Ag/AgCl), which is close to

Table 1
Analytical performance of lactate determination in different real samples.

Sample	Determined by CN-CHMC/LOx (μM)	Added (μM)	Found (μM)	Mean recovery (%)
Soft drink	31.8	0	31.8	N/A
		30	62.8	103.3
		60	93.4	102.6
		90	123.7	102.1
Human sweat	173.2	0	173.2	N/A
		180	349.3	97.8
		360	537.0	101.1
		540	695.5	96.7

the potential of type I Cu site of BOx reported in literatures [54,55]. These results clearly indicate that the catalytic current responses are due to the direct electron transfer-type bioelectrocatalytic feature of BOx for O_2 reduction at BOx-based biocathode.

Taking into account that the CN-CHMC/LOx-TTF and BOx-based biocathode exhibit delightful properties for lactate oxidation and O_2 reduction, respectively, high-performance lactate/air BFC can be assembled. Fig. 5D exhibits the schematic of assembled lactate/air BFC. Bioanodic catalyst LOx oxidizes the lactate mediated by TTF, and generated electrons and protons are transferred from CN-CHMC/LOx-TTF bioanode to the BOx-based biocathode through an external circuit and an internal electrolyte, respectively. At the biocathode, the biocathodic catalyst BOx directly reduces oxygen. In the presence of lactate, the onset potential at the CN-CHMC/LOx-TTF bioanode for lactate electrooxidation is lower than that at the BOx-based biocathode for O_2 reduction, which allows current spontaneously generate based on the galvanic cell principle [56]. Fig. 5E displays the performance of the assembled lactate/air BFCs with CN-CHMC-based and CNT-based bioanodes in air-saturated solution containing 50 mM lactate. The open circuit potential (OCP) of BFC with CN-CHMC-based bioanode (0.65 V) is almost similar to that of BFC with CNT-based bioanode (0.64 V). However, the maximum power density (P_{max}) of BFC with CN-CHMC-based bioanode is 112.7 μW cm^{-2}, which is higher than that on BFC with CNT-based bioanode of 98.3 μW cm^{-2}. It is noteworthy that the P_{max} of BFC with CN-CHMC-based bioanode (112.7 μW cm^{-2}) is not only larger than that of BFC with CNT-based bioanode, but also comparable or even superior than that of other reported lactate/air BFC (Table S3), such as dimethylferrocene-modified linear polyethylenimine/LOx bioanode-based lactate BFC (61.2 μW cm^{-2}) [57] and Nafion/LOx/CNT based-based lactate BFC (24.43 μW cm^{-2}) [58].

Wearable or portable electronic devices have attracted interest from academia and industry due to their applications in biomedicine, security, environment, soft robotics and communications [59,60]. Although advances in functional materials and manufacturing technologies have greatly facilitated the development of these devices, many of them still need to be equipped with traditional systems, such as lithium-ion batteries that require external charging and are not user-friendly [19,26]. A promising alternative is to use BFCs that generate green electricity from widely available samples [7,26]. As described above, lactate can be widely found in biofluids, so lactate-containing human sweat is a potential biofuel for wearable electronic devices [61,62]. As a fermentation product, lactate widely exists in many fermented products, so lactate-containing soft drinks are also considered suitable fuels for portable electronic devices due to their green, available and low-cost properties. Fig. 5F displays the performance of lactate BFCs by adopting the mixture of real samples (commercial soft drink and human sweat) and air-saturated PBS with a volume ratio of 1:4 (v:v) as fuels. When human sweat or soft drink is employed as the fuel of lactate BFC, the corresponding power generation is 23.6 μW cm^{-2} or 31.2 μW cm^{-2}. The different lactate/air BFC powers from real samples are attributed to the different lactate concentrations in the sample, which can be observed from Table 1. The results demonstrate that the assembled lactate BFC is capable of generating electricity from the multi-component sample.

2.5. Cost analysis to CN-CHMC

Besides outstanding electrochemical activities, the feedstock cost is considered as a significant factor as it is closely related to the feasibility of large-scale applications. The feedstock cost of CN-CHMC is down to ~US$ 0.58 g^{-1}, which is much lower than that of commercial CNT (US$ 1688.81 g^{-1}) or graphene (US$ 1517.3 g^{-1}), demonstrating an attractive cost-saving feature of the CN-CHMC (Table S4).

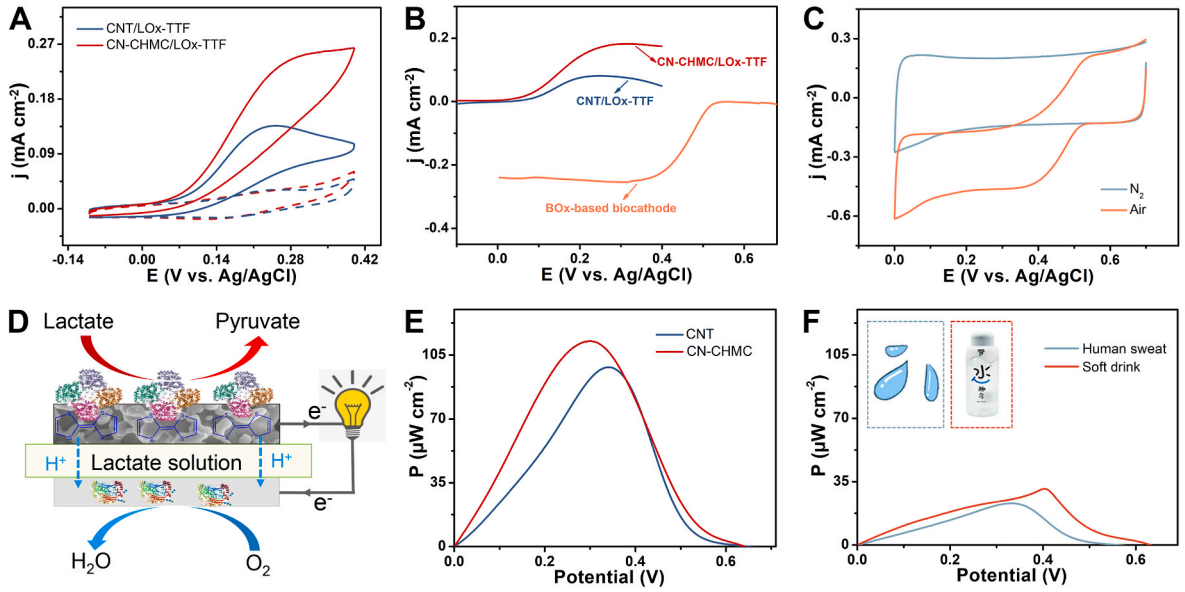

Fig. 5. (A) CVs of CN-CHMC/LOx-TTF and CNT/LOx-TTF in the presence of 50 mM lactate. Dotted lines: background responses. Scan rate: 5 mV s^{-1}. (B) Background-subtracted polarization curves of CN-CHMC/LOx-TTF and CNT/LOx-TTF toward 50 mM lactate oxidation. The curve of biocathode toward O_2 reduction is also shown. Scan rate: 2 mV s^{-1}. (C) CVs of biocathode in N_2-saturated and air-saturated 0.1 M pH 7.0 PBS. Scan rate: 5 mV s^{-1}. (D) Schematic of the designed lactate/air BFC. (E) Power output characteristics of lactate/air BFCs equipped with CNT-based and CN-CHMC-based bioanodes. Electrolyte: air-saturated 0.1 M pH 7.0 PBS containing 50 mM lactate. (F) Power output characteristics of lactate/air BFCs harvesting energy from human sweat and soft drink. Scan rate in E–F: 2 mV s^{-1}.

3. Conclusions

A novel and low-cost carbon material, CN-CHMC, was synthesized, characterized, and used as electrode substrates to construct high-performance lactate biosensor and BFC. The CN-CHMC with abundant defective sites and porous structure may facilitate the high-mass loading of enzymes and provide unobstructed channels for the penetration and transportation of species, which are beneficial to accelerate electron transfer. Taking advantage of its excellent electrochemical reactivity, the CN-CHMC-based lactate biosensor was fabricated and shows satisfactory biosensing performance. In addition, a one-compartment lactate/air BFC was also fabricated by combining CN-CHMC-based bioanode for oxidizing lactate and BOx-based biocathode for reducing oxygen. The feasibility of the lactate/air BFC in practical application is demonstrated by harvesting electrical energy from real samples. Conclusionally, the current studies demonstrate that the introduction of CN-CHMC may open up a new direction in developing high-performance bioelectrochemical devices.

CRediT authorship contribution statement

Cuixing Xu: Conceptualization, Investigation, Methodology, Formal analysis, Data curation, Writing – original draft, Writing – review & editing, Validation. **Gangyong Li:** Methodology, Conceptualization, Investigation, Formal analysis, Writing – original draft, Writing – review & editing, Data curation, Validation. **Ming Zhou:** Conceptualization, Formal analysis, Writing – original draft, Writing – review & editing, Supervision. **Zongqian Hu:** Conceptualization, Resources, Writing – original draft, Writing – review & editing, Formal analysis, Supervision, Project administration, Funding acquisition.

Declaration of competing interest

The authors declare that they have no known competing financial interests or personal relationships that could have appeared to influence the work reported in this paper.

Acknowledgements

The authors would like to acknowledge the support from the National Natural Science Foundation of China (81871506, 81301345), the Jilin Provincial Department of Education (China), the Key Laboratory of Nanobiosensing and Nanobioanalysis at Universities of Jilin Province (China), and the Analysis and Testing Center of Northeast Normal University (China).

Appendix A. Supplementary data

Supplementary data to this article can be found online at https://doi.org/10.1016/j.aca.2022.339994.

References

[1] X. Xuan, C. Pérez-Ràfols, C. Chen, M. Cuartero, G.A. Crespo, Lactate biosensing for reliable on-body sweat analysis, ACS Sens. 6 (2021) 2763–2771.
[2] U.B. Gunatilake, S. Garcia-Rey, E. Ojeda, L. Basabe-Desmonts, F. Benito-Lopez, TiO_2 nanotubes alginate hydrogel scaffold for rapid sensing of sweat biomarkers: lactate and glucose, ACS Appl. Mater. Interfaces 13 (2021) 37734–37745.
[3] P. Giménez-Gómez, M. Gutiérrez-Capitán, F. Capdevila, A. Puig-Pujol, C. Fernández-Sánchez, C. Jiménez-Jorquera, Monitoring of malolactic fermentation in wine using an electrochemical bienzymatic biosensor for l-lactate with long term stability, Anal. Chim. Acta 905 (2016) 126–133.
[4] R.A. Escalona-Villalpando, R.C. Reid, R.D. Milton, L. Arriaga, S.D. Minteer, J. Ledesma-García, Improving the performance of lactate/oxygen biofuel cells using a microfluidic design, J. Power Sources 342 (2017) 546–552.
[5] H. Cheng, C. Hu, Z. Ji, W. Ma, H. Wang, A solid ionic lactate biosensor using doped graphene-like membrane of Au-EVIMC-titania nanotubes-polyaniline, Biosens. Bioelectron. 118 (2018) 97–101.
[6] J. Huang, Y. Zhang, F. Ding, D. Chen, Y. Wang, X. Jin, X. Zhu, Rational design of electroactive redox enzyme nanocapsules for high-performance biosensors and enzymatic biofuel cell, Biosens. Bioelectron. 174 (2021), 112805.
[7] L. Wang, X. Wu, B.Q.w. Su, R. Song, J.-R. Zhang, J.-J. Zhu, Enzymatic biofuel cell: opportunities and intrinsic challenges in futuristic applications, Adv. Energy Sustainability Res. 2 (2021), 2100031.
[8] D.P. Hickey, R.C. Reid, R.D. Milton, S.D. Minteer, A self-powered amperometric lactate biosensor based on lactate oxidase immobilized in dimethylferrocene-modified LPEI, Biosens. Bioelectron. 77 (2016) 26–31.
[9] K. Hiraka, K. Kojima, W. Tsugawa, R. Asano, K. Ikebukuro, K. Sode, Rational engineering of *Aerococcus viridans* L-lactate oxidase for the mediator modification to achieve quasi-direct electron transfer type lactate sensor, Biosens. Bioelectron. 151 (2020), 111974.
[10] X. Jia, S. Dong, E. Wang, Engineering the bioelectrochemical interface using functional nanomaterials and microchip technique toward sensitive and portable electrochemical biosensors, Biosens. Bioelectron. 76 (2016) 80–90.
[11] S. Cosnier, A.J. Gross, A. Le Goff, M. Holzinger, Recent advances on enzymatic glucose/oxygen and hydrogen/oxygen biofuel cells: achievements and limitations, J. Power Sources 325 (2016) 252–263.
[12] Y. Gao, Y. Zeng, X. Liu, D. Tang, Liposome-mediated in situ formation of type-I heterojunction for amplified photoelectrochemical immunoassay, Anal. Chem. 94 (2022) 4859–4865.
[13] J. Shu, D. Tang, Recent advances in photoelectrochemical sensing: from engineered photoactive materials to sensing devices and detection modes, Anal. Chem. 92 (2020) 363–377.
[14] T. Hong, W. Liu, M. Li, C. Chen, Recent advances in the fabrication and application of nanomaterial-based enzymatic microsystems in chemical and biological sciences, Anal. Chim. Acta 1067 (2019) 31–47.
[15] C.H. Kwon, S.-H. Lee, Y.-B. Choi, J.A. Lee, S.H. Kim, H.-H. Kim, G.M. Spinks, G. G. Wallace, M.D. Lima, M.E. Kozlov, High-power biofuel cell textiles from woven biscrolled carbon nanotube yarns, Nat. Commun. 5 (2014) 1–7.
[16] L. Wang, Y. Wang, Y. Qiao, S. Wu, X. Lu, J.-J. Zhu, J.-R. Zhang, H. Zhou, Superior efficient rechargeable lithium-air batteries using a bifunctional biological enzyme catalyst, Energy Environ. Sci. 13 (2020) 144–151.
[17] C. Xu, J. Liu, Y. Bi, C. Ma, J. Bai, Z. Hu, M. Zhou, Biomass derived worm-like nitrogen-doped-carbon framework for trace determination of toxic heavy metal lead (II), Anal. Chim. Acta 1116 (2020) 16–26.
[18] C. Xu, G. Li, Y. Ning, M. Zhou, Z. Hu, Banana peel derived nitrogen-doped porous carbon with enhanced electrocatalytic activity for complete oxidation of methanol under room temperature, Sens. Actuators, B 344 (2021), 130112.
[19] R. Zeng, Z. Luo, L. Zhang, D. Tang, Platinum nanozyme-catalyzed gas generation for pressure-based bioassay using polyaniline nanowires-functionalized graphene oxide framework, Anal. Chem. 90 (2018) 12299–12306.
[20] J. Shu, Z. Qiu, D. Tang, Self-referenced smartphone imaging for visual screening of H_2S using CuxO-polypyrrole conductive aerogel doped with graphene oxide framework, Anal. Chem. 90 (2018) 9691–9694.
[21] A.M. Abioye, F.N. Ani, Recent development in the production of activated carbon electrodes from agricultural waste biomass for supercapacitors: a review, Renew. Sustain. Energy Rev. 52 (2015) 1282–1293.
[22] J. Zhou, S. Zhang, Y.-N. Zhou, W. Tang, J. Yang, C. Peng, Z. Guo, Biomass-derived carbon materials for high-performance supercapacitors: current status and perspective, Electrochem. Energy Rev. 4 (2021) 219–248.
[23] G. Li, Z. Li, X. Xiao, Y. An, W.A. Wang, Z. Hu, An ultrahigh electron-donating quaternary-N-doped reduced graphene oxide@ carbon nanotube framework: a covalently coupled catalyst support for enzymatic bioelectrodes, J. Mater. Chem. 7 (2019) 11077–11085.
[24] S. Zhang, S.-F. Jiang, B.-C. Huang, X.-C. Shen, W.-J. Chen, T.-P. Zhou, H.-Y. Cheng, B.-H. Cheng, C.-Z. Wu, W.-W. Li, Sustainable production of value-added carbon nanomaterials from biomass pyrolysis, Nat. Sustain. 3 (2020) 753–760.
[25] A. Gopalakrishnan, S. Badhulika, Ultrathin graphene-like 2D porous carbon nanosheets and its excellent capacitance retention for supercapacitor, J. Ind. Eng. Chem. 68 (2018) 257–266.
[26] M. Sun, Y. Gu, X. Pei, J. Wang, J. Liu, C. Ma, J. Bai, M. Zhou, A flexible and wearable epidermal ethanol biofuel cell for on-body and real-time bioenergy harvesting from human sweat, Nano Energy 86 (2021), 106061.
[27] M. Sun, T. Xin, Z. Ran, X. Pei, C. Ma, J. Liu, M. Cao, J. Bai, M. Zhou, A bendable biofuel cell-based fully integrated biomedical nanodevice for point-of-care diagnosis of scurvy, ACS Sens. 6 (2021) 275–284.
[28] X. Liu, Y. Zhou, W. Zhou, L. Li, S. Huang, S. Chen, Biomass-derived nitrogen self-doped porous carbon as effective metal-free catalysts for oxygen reduction reaction, Nanoscale 7 (2015) 6136–6142.
[29] L. Zhu, Y. Wang, Y. Wang, L. You, X. Shen, S. Li, An environmentally friendly carbon aerogels derived from waste pomelo peels for the removal of organic pollutants/oils, Microporous Mesoporous Mater. 241 (2017) 285–292.
[30] L. Zeng, X. Li, S. Fan, J. Mu, M. Qin, X. Wang, G. Gan, M. Tadé, S. Liu, Seaweed-derived nitrogen-rich porous biomass carbon as bifunctional materials for effective electrocatalytic oxygen reduction and high-performance gaseous toluene absorbent, ACS Sustain. Chem. Eng. 7 (2019) 5057–5064.
[31] Y. Song, X. Lu, Y. Li, Q. Guo, S. Chen, L. Mao, H. Hou, L. Wang, Nitrogen-doped carbon nanotubes supported by macroporous carbon as an efficient enzymatic biosensing platform for glucose, Anal. Chem. 88 (2016) 1371–1377.
[32] M. Zhou, L. Shang, B. Li, L. Huang, S. Dong, The characteristics of highly ordered mesoporous carbons as electrode material for electrochemical sensing as compared with carbon nanotubes, Electrochem. Commun. 10 (2008) 859–863.

[33] N. Jia, Z. Wang, G. Yang, H. Shen, L. Zhu, Electrochemical properties of ordered mesoporous carbon and its electroanalytical application for selective determination of dopamine, Electrochem. Commun. 9 (2007) 233–238.
[34] B.Y. Xia, Y. Yan, N. Li, H.B. Wu, X.W. Lou, X. Wang, A metal–organic framework-derived bifunctional oxygen electrocatalyst, Nat. Energy 1 (2016) 15006.
[35] Y. Hei, X. Li, X. Zhou, J. Liu, M. Hassan, S. Zhang, Y. Yang, X. Bo, H.-L. Wang, M. Zhou, Cost-effective synthesis of three-dimensional nitrogen-doped nanostructured carbons with hierarchical architectures from the biomass of sea-tangle for the amperometric determination of ascorbic acid, Anal. Chim. Acta 1029 (2018) 15–23.
[36] N. Wang, Y. Hei, J. Liu, M. Sun, T. Sha, M. Hassan, X. Bo, Y. Guo, M. Zhou, Low-cost and environment-friendly synthesis of carbon nanorods assembled hierarchical meso-macroporous carbons networks aerogels from natural apples for the electrochemical determination of ascorbic acid and hydrogen peroxide, Anal. Chim. Acta 1047 (2019) 36–44.
[37] C. Xu, Y. Hei, J. Liu, M. Sun, T. Sha, N. Wang, M. Hassan, X. Bo, M. Zhou, Synthesis of a three-dimensional interconnected carbon nanorod aerogel from wax gourd for amperometric sensing, Microchim. Acta 185 (2018) 482.
[38] R.C. Cui, B. Xu, H.J. Dong, C.C. Yang, Q. Jiang, N/O dual-doped environment-friendly hard carbon as advanced anode for potassium-ion batteries, Adv. Sci. 7 (2020), 1902547.
[39] G. Li, G. Ren, W.A. Wang, Z. Hu, Rational design of N-doped CNTs@C_3N_4 network for dual-capture of biocatalysts in enzymatic glucose/O_2 biofuel cells, Nanoscale 13 (2021) 7774–7782.
[40] Y. Wang, Y. Shao, D.W. Matson, J. Li, Y. Lin, Nitrogen-doped graphene and its application in electrochemical biosensing, ACS Nano 4 (2010) 1790–1798.
[41] H. Tao, C. Yan, A.W. Robertson, Y. Gao, J. Ding, Y. Zhang, T. Ma, Z. Sun, N-doping of graphene oxide at low temperature for the oxygen reduction reaction, Chem. Commun. 53 (2017) 873–876.
[42] C.X. Guo, F.P. Hu, X.W. Lou, C.M. Li, High-performance biofuel cell made with hydrophilic ordered mesoporous carbon as electrode material, J. Power Sources 195 (2010) 4090–4097.
[43] D.A. Aikens, Electrochemical methods, fundamentals and applications, J. Chem. Educ. 60 (1983) A25.
[44] Y. Bi, Y. Hei, N. Wang, J. Liu, C.-B. Ma, Synthesis of a clustered carbon aerogel interconnected by carbon balls from the biomass of taros for construction of a multi-functional electrochemical sensor, Anal. Chim. Acta 1164 (2021), 338514.
[45] A.F. Quintero-Jaime, J. Quílez-Bermejo, D. Cazorla-Amorós, E. Morallón, Metal free electrochemical glucose biosensor based on N-doped porous carbon material, Electrochim. Acta 367 (2021), 137434.
[46] S.-J. Bao, C.M. Li, J.-F. Zang, X.-Q. Cui, Y. Qiao, J. Guo, New nanostructured TiO_2 for direct electrochemistry and glucose sensor applications, Adv. Funct. Mater. 18 (2008) 591–599.
[47] Dhanjai, X. Lu, L. Wu, J. Chen, Y. Lu, Robust single-molecule enzyme nanocapsules for biosensing with significantly improved biosensor stability, Anal. Chem. 92 (2020) 5830–5837.
[48] M.R. Romero, F. Ahumada, F. Garay, A.M. Baruzzi, Amperometric biosensor for direct blood lactate detection, Anal. Chem. 82 (2010) 5568–5572.
[49] M. Janyasupab, C.-W. Liu, N. Chanlek, S. Chio-Srichan, C. Promptmas, W. Surareungchai, A comparative study of non-enzymatic glucose detection in artificial human urine and human urine specimens by using mesoporous bimetallic cobalt-iron supported N-doped graphene biosensor based on differential pulse voltammetry, Sens. Actuators, B 286 (2019) 550–563.
[50] J. Scremin, E.C.M. Barbosa, C.A.R. Salamanca-Neto, P.H.C. Camargo, E.R. Sartori, Amperometric determination of ascorbic acid with a glassy carbon electrode modified with TiO_2-gold nanoparticles integrated into carbon nanotubes, Microchim. Acta 185 (2018) 251.
[51] E. Asav, E. Akyilmaz, Preparation and optimization of a bienzymic biosensor based on self-assembled monolayer modified gold electrode for alcohol and glucose detection, Biosens. Bioelectron. 25 (2010) 1014–1018.
[52] H. Liu, J. Deng, An amperometric lactate sensor employing tetrathiafulvalene in Nafion film as electron shuttle, Electrochim. Acta 40 (1995) 1845–1849.
[53] K. So, S. Kawai, Y. Hamano, Y. Kitazumi, O. Shirai, M. Hibi, J. Ogawa, K. Kano, Improvement of a direct electron transfer-type fructose/dioxygen biofuel cell with a substrate-modified biocathode, Phys. Chem. Chem. Phys. 16 (2014) 4823–4829.
[54] K. Murata, K. Kajiya, N. Nakamura, H. Ohno, Direct electrochemistry of bilirubin oxidase on three-dimensional gold nanoparticle electrodes and its application in a biofuel cell, Energy Environ. Sci. 2 (2009) 1280–1285.
[55] M. Zhao, Y. Gao, J. Sun, F. Gao, Mediatorless glucose biosensor and direct electron transfer type glucose/air biofuel cell enabled with carbon nanodots, Anal. Chem. 87 (2015) 2615–2622.
[56] Encyclopedia of Electrochemical Power Sources, Elsevier, Amsterdam, 2009.
[57] R.A. Escalona-Villalpando, R.C. Reid, R.D. Milton, L.G. Arriaga, S.D. Minteer, J. Ledesma-García, Improving the performance of lactate/oxygen biofuel cells using a microfluidic design, J. Power Sources 342 (2017) 546–552.
[58] K. Wang, L. Du, Q. Wei, J. Zhang, G. Zhang, W. Xing, S. Sun, A lactate/oxygen biofuel cell: the coupled lactate oxidase anode and PGM-free Fe-N-C cathode, ACS Appl. Mater. Interfaces 11 (2019) 42744–42750.
[59] Q. Zhang, Z. Zhang, Q. Liang, F. Gao, F. Yi, M. Ma, Q. Liao, Z. Kang, Y. Zhang, Green hybrid power system based on triboelectric nanogenerator for wearable/portable electronics, Nano Energy 55 (2019) 151–163.
[60] J. Tu, R.M. Torrente-Rodríguez, M. Wang, W. Gao, The era of digital health: a review of portable and wearable affinity biosensors, Adv. Funct. Mater. 30 (2020), 1906713.
[61] W. Jia, G. Valdés-Ramírez, A.J. Bandodkar, J.R. Windmiller, J. Wang, Epidermal biofuel cells: energy harvesting from human perspiration, Angew. Chem. Int. Ed. 52 (2013) 7233–7236.
[62] E. Ortiz-Ortega, R. Escalona-Villalpando, J.D.D. Galindo de la Rosa, J. Ledesma-García, S. Minteer, L.G. Arriaga, Sweat as energy source using an enzymatic microfluidic fuel cell, J.Phys. Conf. Ser. 1052 (2018), 012142.